Nuclear Instruments and Methods in Physics Research A 829 (2016) 408–412

Contents lists available at ScienceDirect

Nuclear Instruments and Methods in Physics Research A

journal homepage: www.elsevier.com/locate/nima

Comparison of self-injection thresholds in He and N_2 and role of self-focusing in LWFA

D. Palla [a,b,*], F. Baffigi [a], F. Brandi [a,c], L. Fulgentini [a], P. Koester [a], L. Labate [a,b], P. Londrillo [d], L.A. Gizzi [a,b]

[a] Intenser Laser Irradiation Laboratory, INO-CNR, Via Moruzzi, 1 56124 Pisa, Italy
[b] INFN, Sez. Pisa, Largo B. Pontecorvo, 3 - 56127 Pisa, Italy
[c] Istituto Italiano di Tecnologia, Nanophysics Department, via Morego 30, 16163 Genova, Italy
[d] Universitá di Bologna e Sez. INFN, Bologna, Italy

ARTICLE INFO

Article history:
Received 30 November 2015
Received in revised form
13 March 2016
Accepted 31 March 2016
Available online 16 April 2016

Keywords:
Self injection
Ionization
LWFA
Self focusing

ABSTRACT

We present an experimental study of laser-plasma acceleration in which the injected charge was measured at self-injection threshold for He and N_2. We use numerical particle-in-cell simulation to unfold the role of ionization in the self-injection process and to reconstruct the local electrons density from the atomic density and the ionization degree. Comparison of measured and calculated self-injection thresholds yields the dependence of injected charge upon the electron density and sheds light on the possible role of the picosecond pedestal of femtosecond laser pulses in setting the initial charge state of the plasma.

1. Introduction

In their original paper, Tajima and Dawson [1] suggest to use the wakefield generated by an intense laser pulse to accelerate electron to relativistic energies. After many years, high-power laser pulses with a suitable femtosecond duration have been developed and are available in many laboratories. Laser Wakefield Acceleration (LWFA) has been extensively explored and impressive results have been obtained wordwide [2,3] showing electron energies up to 4 GeV [4]. More recently, staging of two LWFA accelerators has been demonstrated experimentally [5]. In LWFA, the high longitudinal electric field supported by the plasma wave is used to accelerate trapped (self-injected) electrons with velocity close to wave phase velocity. With respect to the standard RF-linacs, the accelerating gradient of LWFA is much higher, leading to relativistic electron beams over impressively small distances (in principle, 1000 times shorter). Recently, LWFA has been proposed as source of high energy electrons to drive generation of high energy radiation using secondary processes like bremsstrahlung, betatron and Thomson/Compton scattering [6,7]. At the same time, great attention is being dedicated to the possible use of LWFA as a source of high energy particles for radiobiology and radiation therapy [8].

Control of the self-injection of electrons in the accelerating structure is currently considered a crucial step for the achievement of reproducible and reliable acceleration using LWFA. In this context, the dynamics of ionization of the atoms in the gas target plays a key role in both the propagation of laser pulse [9] and the self-injection of electrons [10]. Mixtures of low-Z gas containing a small percentage of higher-Z gas with a large gap between successive ionization potentials have been demonstrated [11] to provide more effective and controllable injection. In this way, quality and stability of LWFA accelerated electron can be improved by using the so-called “ionization injection” [11–13]. This process occurs when the laser intensity is such that additional field ionization of the inner shell electrons of the target atoms only occurs at the peak of the pulse, modifying significantly the electron injection dynamics. More recently, additional techniques have been proposed [14,15] to limit the large energy spread typical of accelerated electrons originating from ionization injection. Typically this regime requires a minimum normalized laser field $a_0 \simeq 1.7$ [16].

Besides the specific ionization injection conditions, ionization of the gas atoms plays a role in setting the initial evolution of plasma [17] in the gas and the phase space distribution of free electrons. For typical relativistic laser intensity ($\geq 10^{18}$W/cm^2) this process is dominated by tunneling ionization. Usually, for low-Z

* Corresponding author at: Intenser Laser Irradiation Laboratory, INO-CNR, Via Moruzzi, 1 56124 Pisa, Italy.

http://dx.doi.org/10.1016/j.nima.2016.03.109
0168-9002/

gas (H, He) and outer shells of high-Z gas, ionization occurs very early during the laser pulse or even in the ps laser pedestal that can fully ionize the target before the main pulse arrives. Unlike the case of ionization injection, in the latter case the ionization process has little effect on the injection of electrons and on the wakefield acceleration process. Therefore, the understanding of the actual role of ionization in a given experimental configuration is a complex task and requires a dedicated investigation.

In this paper we investigate experimentally the effects of ionization on self-injection threshold and the dependence of the injected charge upon the initial atomic density for pure He and pure N_2 to quantify the role of ionization in the injection process in our experimental conditions and to retrieve, via comparison with numerical simulations, the actual charge state of N_2 atoms in the injection region.

2. Experimental setup

The experiment was performed at the Intense Laser Irradiation Laboratory (ILIL) in Pisa using the 10 TW Ti:Sa laser system. The infrared ($\lambda_0 = 800$ nm) laser system delivers 40 fs (at FWHM) pulse up to 450 mJ on target. The linearly p-polarized laser pulse is focused using a $f/10$ off-axis parabola down to 20 μm diameter (FWHM) focal spot. The corresponding maximum intensity on target was up to 2×10^{18} W/cm^2 with a normalized vector potential $a_0 = eE_L/m_e\omega_L c$ equal to 0.96. The beam was focused onto a laminar supersonic gas-jet produced using a 1.2×4 mm^2 rectangular nozzle, with the laser propagating across the shortest side. Here we show results obtained with He and N_2.

The gas-jet density profile was measured by using interferometric techniques to obtain the dependence of atom density distribution upon the backing pressure in order to use a realistic density profile in PIC modeling. The N_2 and He backing pressure used in our experiment ranged respectively from 2.5 to 5 bar and from 12 to 20 bar. These pressures correspond to maximum atomic densities of $1 - 2 \times 10^{18}$ atoms/cm^3 for N_2 and $2.4 - 4 \times 10^{18}$ atoms/cm^3 for He.

A linear dependence of atomic density upon backing pressure was found with coefficient of 2×10^{17} molecules/(cm^3 bar). Gas jet profile is characterized by 1.2 mm long uniform central density region and 0.2 mm linearly decreasing regions (ramps) at the edges (0.2 + 1.2 + 0.2 mm in total). No relevant difference in gas-jet profile was observed in 2.5–20 bar range of backing pressure.

The laser was focused about 0.1 mm before the entrance of the gas-jet, at the middle of initial density ramp and lead to the formation of roughly 1.5 mm long plasma channel. The laser-gas interaction was monitored using Thomson scattering imaging and shadowgraphy with a frequency doubled (400 nm) probe pulse. A 40 μm thick Mylar window was used to extract accelerated electrons from the vacuum chamber. The spatial profile of the accelerated electron beam was monitored using a Regular Lanex scintillating screen mounted just outside the interaction chamber at a total distance of about 45 cm from the gas-jet. The Lanex screen was image out by a standard camera lens onto a cooled EMCCD (Andor). For measuring electron energy spectra a magnetic dipole was inserted on the electron transport line 9 cm before the scintillating screen; the field strength and the dipole to scintillator screen were chosen so as to optimize the energy resolution in the range 5–40 MeV.

3. Experimental results

We measured the injected charge at different gas densities. For this purpose He and N_2 were used in the very same interaction condition, including the laser focus position with respect to the gas-jet. The atomic density was varied changing the gas-jet backing pressure. A signal proportional to the injected charge was obtained by measuring the integrated electron signal over a surface of 15×7 cm of the Lanex screen which contains the entire injected electron beam. The explored atomic density range of $1 - 4 \times 10^{18}$ atoms/cm^3 includes self-injection threshold for both He and N_2. Fig. 1 shows the dependence of the measured charge (in arbitrary units) as a function of the atomic gas density. We immediately observe several differences between N_2 and He interaction

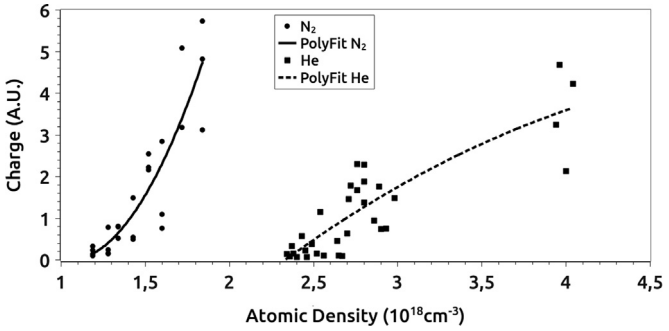

Fig. 1. Experimental measurement of the injected charge as a function of the atomic density. A fit with a degree 2 polynomial function is also showed.

1. The injected charge shows a different dependence upon the initial atomic density for He and N_2. In particular N_2 shows a quadratic dependence around injection threshold while He shows a nearly linear behaviour.
2. Assuming a maximum ionization of N^{5+} for N_2 and full ionization for He (these point will be deepened later), we find that ionization density thresholds are respectively 6×10^{18} cm^{-3} vs 4.5×10^{18} cm^{-3} which are significantly different.
3. Helium shows a poor shot to shot stability just around the self-injection threshold: $2.4 - 2.7 \times 10^{18}$ cm^{-3}. Threshold is less well defined with respect to the N_2 case.

4. Numerical simulations

In order to get more information about the injection and acceleration dynamic in this regime we carried out several 2-D simulation using the fully self-consistent PIC code Jasmine [18]. To support the results here presented, a crosscheck with a different code AlaDyn [19] was also performed. In both codes the ionization process is modelled using the ADK model [20]. The simulations are performed using a resolution of $\Delta x = 0.03\lambda_0$, $\Delta y = 0.12\lambda_0$ with the laser propagating along x-axis. We carried out numerical density scans in the same interaction conditions used in the experiment, including the gas-jet profile. The numerical results plotted in Fig. 2 show some remarkable similarity with the experimental results. First of all, despite the limited 2-D nature of simulation, injection threshold for N_2 (1.2×10^{18} cm^{-3}) is really close to the experimental one (1.3×10^{18} cm^{-3}). In addition to this, the dependence of the injected charge upon the atomic density is different from He to N_2 and shows a similar trend to the experimental curve. In particular N_2 shows a moderate quadratic-like profile. In contrast, we observe that calculated density threshold for He is quite different from the experimental one (3.7×10^{18} cm^{-3} vs 2.4×10^{18} cm^{-3} respectively). These preliminary observations suggest that a deeper analysis is required to understand the different phenomenology occurring in He and N_2.

Preliminarily it is useful to recall the ionization potentials for

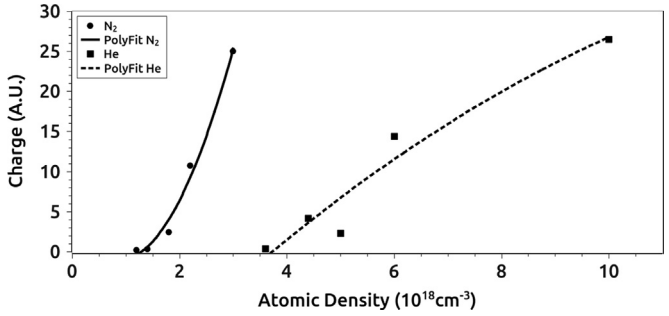

Fig. 2. Injected charge is retrieved by PIC simulation as a function of atomic density. A fit with a degree 2 polynomial function is also showed.

one level transition $N \rightarrow N^{+}$, up to $N^{6+} \rightarrow N^{7+}$ which are 14.534, 29.601, 47.449, 77.472, 97.888, 552.057 and 667.029 eV respectively. Usually, to implement ionization injection, $N^{5+} \rightarrow N^{6+}$ is used [16] due to the large difference in ionization potential with respect to the previous one.

In our experimental configuration, according to the ADK model, laser intensity is strong enough to ionize the nitrogen up the N^{5+} level, with a notable contribution of N^{6+}. The ionization degree of N_2 after 1.2 mm of propagation (at 2.26×10^{18} cm^{-3} atomic density) is shown in Fig. 3. As we can see, on the laser axis, where the intensity is higher, a N^{6+} contribution is present. The influence of this contribution depends upon the atomic density and is due to the self-focusing process. We observe that in our experimental conditions, the laser power of 10 TW at 800 nm is greater than the critical power $P_c = 17.5(\omega/\omega_p)^2$ GW for all the explored density values above injection threshold. In fact, the critical electron density corresponding to our laser power is $n_e^{cr} \simeq 3 \times 10^{18}$ cm^{-3} which is smaller than the injection threshold density for both He and N_2. In other word self-focusing is expected to play a role in all our measurements.

These circumstances are fully consistent with PIC simulations which show that, due to self-focusing, the initial values of the normalized laser vector potential $a_0 = 0.96$ can reach, for instance, $a^{max} = 1.6$ or $a^{max} = 1.5$ at 2.2×10^{18} cm^{-3} or 1.8×10^{18} cm^{-3} of atomic density respectively. In Fig. 4 we reported the cumulative probability of ionization from $N^{4+} \rightarrow N^{5+}$, $N^{5+} \rightarrow N^{6+}$ and $N^{6+} \rightarrow N^{7+}$ as a function of laser vector potential calculated used the ADK model. If we compare these curves with our a^{max} values we find that the nitrogen is ionized to N^{5+} well before the peak of the pulse with a further N^{6+} contribution coming only when the

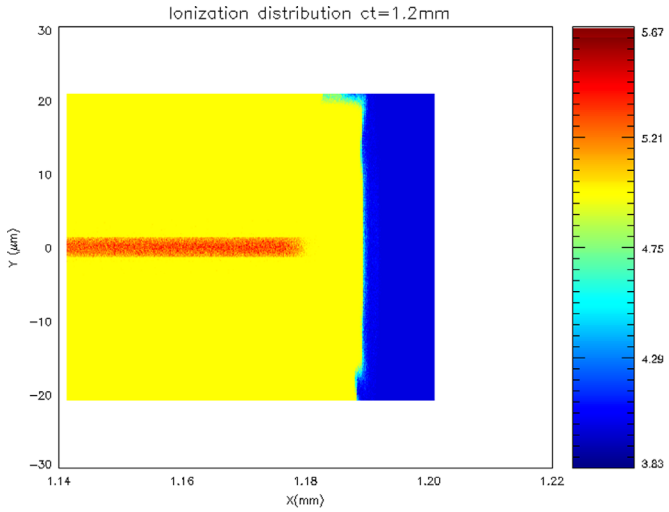

Fig. 3. Ionization degree of N_2 after 1.2 mm of laser propagation at 2.26×10^{18}cm^{-3} atomic density (pre-ionized N^{4+} is considered in this PIC simulation).

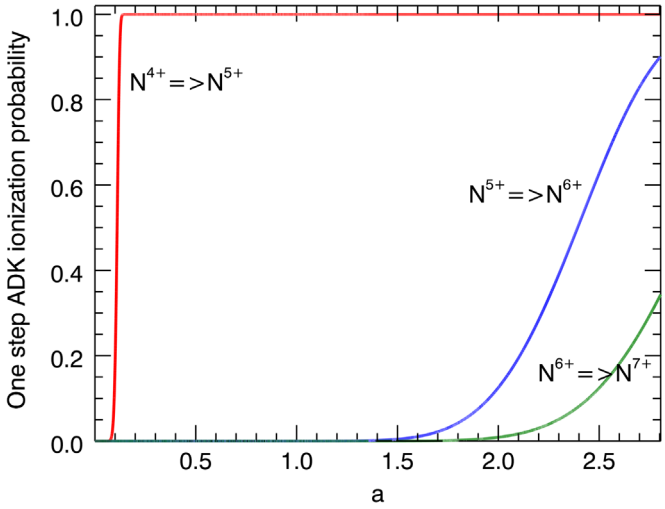

Fig. 4. One step ADK ionization transition probability as a function of normalized potential *a*.

field is fully focused at the peak of the pulse ($a \geq 1.5$). In contrast, helium, with 24.587 eV and 54.417 eV ionization potentials, is 100% ionized well before reaching the peak intensity and over a large longitudinal extent.

In order to understand the different curve trends shown in Fig. 1 we considered the maximum ionization degree of nitrogen at different atomic densities in the numerical simulation. Since particles are injected around the laser axis we can assume that all such particles originate from the region where ionization of N^{6+} is maximum. From the simulations we find that in the $1 - 2.5 \times 10^{18}$ cm^{-3} atomic density range we can approximate the maximum plasma density as:

$$\begin{cases} n_e^{He}(d) = 2 \cdot d, \\ n_e^{N_2}(d) = N^{\#} \cdot d, \end{cases} \quad (1)$$

where d is the atomic density (measured in unity of 10^{18} cm^{-3}) and $N^{\#} = 4.827 + 0.344 \cdot d$ is the average ionization degree for N_2 obtained via simulation. The nitrogen electron density non-linearity is clearly due to the self-focusing effect while He is found to be fully ionized as anticipated above. We additionally point out here that according to PIC simulations, laser depletion around the injection position is negligible in our experimental conditions.

In order to understand if the self-injection process strongly depend upon gas properties we can compare the experimental dependence of injected charge on the plasma density. Using the relation (1) we can express the data shown in Fig. 1 in terms of plasma density. The result is presented in Fig. 5. We consider only the first order difference between He and N_2 and for this reason we can simply consider the linear fit associated to experimental data as shown in Fig. 5. We find that

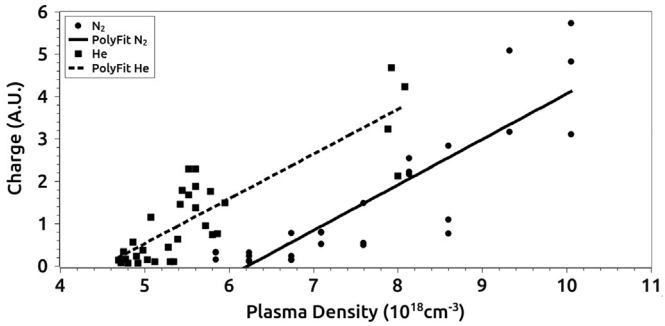

Fig. 5. Experimental data; injected charge dependence on plasma density.

$$\begin{cases} Q_{He}^{exp}(n_e) = -(4.75 \pm 0.43) + (1.056 \pm 0.052)\cdot n_e \\ Q_{N_2}^{exp}(n_e) = -(6.69 \pm 0.46) + (1.075 \pm 0.053)\cdot n_e, \end{cases} \quad (2)$$

where density is measured in unity of 10^{18} cm^{-3}. From Eq. (2) we can easily find the injection threshold, which correspond to:

$$n_e^{exp.th}(He) = (4.49 \pm 0.66) \times 10^{18}\ cm^{-3} \quad (3)$$

for helium and

$$n_e^{exp.th}(N_2) = (6.22 \pm 0.89) \times 10^{18}\ cm^{-3} \quad (4)$$

for N_2.

These results give different injection density thresholds for He and N_2, with Nitrogen showing a significantly higher density. As anticipated before, both thresholds shown in Eqs. (3) and (4) are greater that the critical self-focusing density $n_e^{cr} \simeq 3 \times 10^{18}$ cm^{-3}. These circumstances are not surprising because of the relatively low normalized field $a_0 = 0.96$ which is just below the value required for self-injection without self-focusing [21].

In view of a more detailed discussion of these findings, it is interesting to compare the threshold densities obtained experimentally with the values obtained from PIC simulations.[1] We point out that since we are dealing with 2-D simulations, we do not expect absolute values of the calculated density threshold to be directly comparable with experimental values, while a comparison of the relative values for He and N_2 is more meaningful and may provide useful insight in the injection dynamics. According to the plot of Fig. 2, we obtain the following injection density threshold for He:

$$n_e^{PIC.th}(He) = (7.42 \pm 0.89) \times 10^{18}\ cm^{-3}, \quad (5)$$

and the following for N_2:

$$n_e^{PIC.th}(N_2) = (6.28 \pm 0.82) \times 10^{18}\ cm^{-3}. \quad (6)$$

Numerical simulations indeed predict a slightly smaller density threshold for injection in N_2 compared to He: $(n_e^{PIC.th}(N_2)/n_e^{PIC.th}(He)) \sim 0.85 \pm 0.21$. However, this difference is quite small and if we take into account the statistical error, we can conclude that calculated thresholds for He and for N_2 are basically the same.

This result tells us that, in our experimental conditions and for both gases, ionization is expected to play little or no role in the injection process and the density threshold is simply accounted for by self-focusing. In fact, in the case of He, full ionization is granted at laser intensities well below the peak incident laser intensity, with no need to invoke self-focusing. In the case of N_2, the same is true for ionization up to N^{5+}, while additional contribution from $N^{5+} \rightarrow N^{6+}$ is seen on the laser axis. According to the plot of Fig. 4 , contribution from $N^{5+} \rightarrow N^{6+}$ requires a $a_0 > 1.5$ which can be achieved via self-focusing. According to the relation $N^{\#} = 4.827 + 0.344 \cdot d$ obtained above, by setting $n_e^5 \equiv 5 \cdot d$ corresponding to $N^{\#} = 5$, we find $n_e^5 = 2.5 \times 10^{18}$ cm^{-3} which is the minimum density above which the transition to N^{6+} is expected to contribute to the plasma density. This value is well below the density threshold expected for N_2 (see Eq. (6)), strongly suggesting that contribution of the ionization from $N^{5+} \rightarrow N^{6+}$ to the injection threshold in our case is negligible.

In view of the above considerations, the higher threshold density found for N_2 with respect to He is not predicted by our PIC simulations and may be accounted for by taking into account mechanisms not included in the simulation.

A possible explanation is a contribution from ionization defocusing initiated by precursor laser radiation which is not taken into account in PIC simulations. Precursor radiation relevant here consists [22] of a ps ramp starting approximately 10 ps before the peak of the pulse and reaching an intensity of approximately 10^{-5} of the peak intensity at approximately 0.5 ps before the peak of the pulse, with an intensity on target well above of 10^{13} W/cm^2. In fact, the first electron potential (14.534 eV) in N_2 is significantly lower than the first helium potential (24.587 eV) and the laser prepulse can pre-ionize the nitrogen more than it can pre-ionize helium. The greater susceptibility of N_2 to form preplasma can defocus the laser and reduce the coupling to the plasma wake [11]. Although a quantitative evaluation of this effect is not straightforward and is beyond the scope of this work, we can reasonably assume that ionization defocusing could partially explain the differences in injection threshold of He and N_2 observed experimentally.

One final observation concerns the efficiency of charge trapping. From Eqs. (2) we found that the linear growth of injected charge with electron density is the same for both gases; only ~3% of difference was measured, which is not statistically significant compared to the ~5% error, confirming the negligible role of ionization in the self injection process.

5. Conclusion

We carried out a gas pressure scan of self-injected charge in LWFA to gain information about the self-injection properties of He gas compared to N_2 and identify the possible role of ionization. We refer to a set of experimental parameters relevant for a compact plasma accelerator based on a 10 TW class laser. The measured self-injection density threshold for N_2 is found to be higher than the corresponding threshold for He. In contrast, particle in cell simulations predict a similar threshold for N_2 and He. This prediction is consistent with the ionization process of He and N_2 and the dependence of self-focusing on the plasma density and shows that, in our experimental conditions, ionization of the N^{6+} plays a role at densities well below our self-injection threshold, mainly due to the relatively low laser intensity which requires self-focusing at higher densities. The unexpected higher self-injection threshold for N_2 could be explained taking into account that ionization defocusing initiated by precursor ps laser radiation may play a role due to the lower first ionization potential of N_2 compared to He. This study clearly shows the complex interplay between the different parameters governing the dynamics of self-injection at relatively low laser intensity, due to the crucial role of self-focusing.

Acknowledgments

We acknowledge financial contribution from the ELI-Italy Network funded by the MIUR and from the G-RESIST project of the INFN CN5 and from the italian Ministry of Health through the project GR-2009-1608935 (D.I. AgeNaS).

References

[1] T. Tajima, J.M. Dawson, Phys. Rev. Lett. 43 (1979) 267.
[2] J. Faure, Y. Glinec, A. Pukhov et al., Lett. Nat. 431 (2004) 541.
[3] W.P. Leemans, et al., Nat. Phys. 2 (2006) 696.
[4] W.P. Leemans, et al., Phys. Rev. Lett. 113 (2014) 245002.
[5] S. Steinke, et al., Nature 530 (7589) (2016) 190.
[6] A. Giulietti, et al., Phys. Rev. Lett. 101 (2008) 105002.
[7] S. Chen, et al., Phys. Rev. Lett. 110 (2013) 155003.
[8] L. Labate, et al., Proc. SPIE 8779 (2013) 87790L.
[9] L.A. Gizzi, et al., Phys. Rev. E 74 (2006) 036403.
[10] T.-Y. Chien, et al., Phys. Rev. Lett. 94 (2005) 115003.

[1] The injection threshold is calculated, as for the experimental data, in linear approximation.

[11] A. Pak, et al., Phys. Rev. Lett. 104 (2010) 025003.
[12] M. Chen, Z.-M. Sheng, Y.-Y. Ma, J. Zhang, J. Appl. Phys. 99 (2006) 056109.
[13] C. Mcguffey, et al., Phys. Rev. Lett. 104 (2010) 025004.
[14] M. Mirzaie, et al., Sci. Rep. 5 (2015) 14659.
[15] B. Pollock, et al., Phys. Rev. Lett. 107 (2011) 045001.
[16] M. Chen, et al., Phys. Rev. Lett. 19 (2012) 033101.
[17] L.A. Gizzi, et al., Phys. Rev. E 79 (2009) 056405.
[18] F. Rossi et al., AIP Conf. Proc. 1507, 184 (2012).
[19] C. Benedetti, et al., IEEE Trans. Plasma Sci. 36 (4) (2008) 1790–1798.
[20] M. Chen, et al., J. Comput. Phys. 236 (2013) 220–228.
[21] C. Benedetti, et al., Phys. Plasmas 20 (2013) 103108.
[22] L.A. Gizzi, et al., Nucl. Instrum. Methods A 829 (2016) 144, http://dx.doi.org/10.1016/j.nima.2016.01.036.